ELSEVIER

# Contents lists available at ScienceDirect

# Desalination

journal homepage: www.elsevier.com/locate/desal





# Techno-economic assessment of vertical axis wind turbine driven RO desalination with compressed air energy storage for remote communities

Khalid M. Alzahrani <sup>a,b,\*</sup>, Jee Loong Hee <sup>a</sup>, Mohamed Elsakka <sup>c</sup>, Derek Ingham <sup>a</sup>, Lin Ma <sup>a</sup>, Mohammed Pourkashanian <sup>a</sup>

- a Energy 2050, Department of Mechanical Engineering, Faculty of Engineering, The University of Sheffield, Sheffield, S3 7RD, United Kingdom
- <sup>b</sup> Department of Mechanical Engineering, College of Engineering, Taif University, Taif 21944, Saudi Arabia
- <sup>c</sup> Mechanical Power Dept., Faculty of Engineering, Port Said University, Egypt

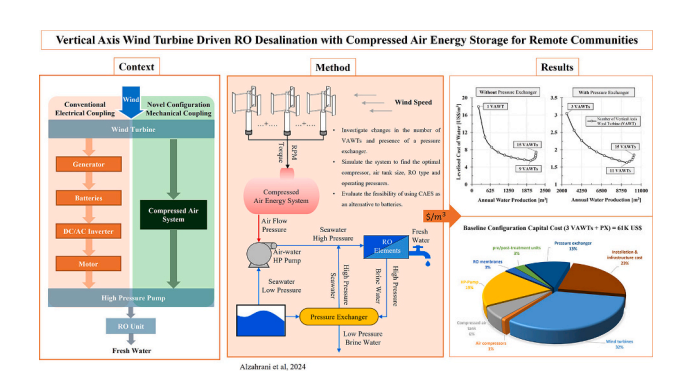
#### HIGHLIGHTS

- Using VAWTs to mechanically drive RO via a compressed air system was investigated.
- Replacement of batteries with compressed air storage reduced water production cost.
- VAWT with a compressed air system is economical, addressing wind intermittency.
- Examined scenarios with varying VAWT numbers with or without energy recovery for the study site.
- Parametric studies resulted in an optimal LCOW of 1.63 US\$/m<sup>3</sup> for an off-grid system.

# ARTICLE INFO

Keywords:
Wind energy
VAWT
Compressed air energy system
SWRO
Techno-economic assessment

#### GRAPHICAL ABSTRACT



# ABSTRACT

Renewable energy desalination is gaining much attention in remote off-grid communities facing challenges in accessing clean water. Typically, batteries ensure the continuous operation of small-scale renewable reverse osmosis (RO) desalination systems; however, they are expensive and have relatively shorter lifespans. This study investigates the implementation of a compressed air energy storage (CAES) system coupled with a vertical axis wind turbine (VAWT) to directly drive small-scale RO desalination, potentially replacing batteries and reducing energy conversions. A Simulink model was developed to simulate the performance of a VAWT-driven CAES operating RO units, adaptable for both technical and economic assessments. Parametric studies have identified the optimal configuration. The most cost-effective configuration, utilising eleven VAWTs and a pressure exchanger (PX), achieves a levelised cost of water (LCOW) of 1.63 US\$/m³ and an annual water production of 9400 m³. The normalised daily water production per square metre of turbine swept area at the study site is 0.19 m³/m²/day at an average wind speed of 5 m/s. While this configuration has a higher initial capital cost, it yields the lowest LCOW. The CAES system effectively addresses the intermittency challenges of wind energy. This study presents a novel, battery-free VAWT-CAES-RO system as a sustainable desalination solution for remote communities, offering a promising approach to address water scarcity in an environmentally friendly manner.

E-mail addresses: kmalzahrani1@sheffield.ac.uk, k.m.alzahrani@tu.edu.sa (K.M. Alzahrani).

#### https://doi.org/10.1016/j.desal.2024.118094

<sup>\*</sup> Corresponding author at: Energy 2050, Department of Mechanical Engineering, Faculty of Engineering, The University of Sheffield, Sheffield, S3 7RD, United Kingdom.

#### 1. Introduction

Water scarcity is a significant global issue affecting both developed and developing countries. It is becoming increasingly apparent due to the rapid population growth, climate change, and droughts [1]. This poses an even greater challenge to many countries geographically situated in some of the world's most arid regions [2]. A UNICEF report revealed that 1.42 billion people struggled to access safe drinking water in 2021, classified as high or extremely high in water vulnerability [3]. Another study projected that 87 out of 180 countries are expected to suffer from water scarcity by 2050 [4]. The main challenge in poor or developing countries is the lack of water infrastructure and the ability to build centralised water desalination to support the community in need of clean water [5]. This highlights the importance of developing small-scale, stand-alone water desalination units.

Seawater (or brackish water) desalination is a promising solution to provide fresh water for coastal areas and communities with access to brackish water wells. While many desalination technologies exist, reverse osmosis (RO) is a commonly used and well-established method in both small- and large-scale water desalination plants [6]. In fact, approximately 69 % of the installed desalination plants globally employ RO [7]. However, the majority of large-scale commercial plants rely on non-renewable energy sources, such as fossil fuels, which contribute to greenhouse gas emissions [8,9]. Therefore, water desalination plants powered by renewable energy are seen as an attractive and viable approach to provide fresh water to communities undergoing such challenges.

Over the past decades, several methods of renewable energy have been proposed and trialled for water desalination [6,7], including wind and solar. Solar desalination can be broadly categorised into solar-powered RO and thermal desalination [10,11]. Wind-powered RO can also be divided into two sub-categories: using electrical energy for battery energy storage (BES) to power the water pump, or direct mechanical pumping to overcome the membrane osmotic pressure [12,13].

Studies have shown that the wind energy powered RO has the lowest water production cost among various mature renewable water desalination technologies [11,14]. This is based on a comparative study of the technology maturity level, specific cost of desalinated water (in \$/m³) and capacity levels [2]. Although, solar multi-effect evaporation (solar-MED) and wave energy RO possess similar metrics in water production (i.e. m³/day) and specific cost of desalinated water, but these technologies are still in the research and development stage as opposed to widespread implementation [2].

Many renewable energy powered RO systems utilise some forms of energy storage to assist with the intermittency of renewable energy sources (e.g. during low wind speeds and fluctuations) to ensure steady operation and water production [14]. Energy storage like batteries, hydro storage and flywheels have been employed in various small-scale pilot plants [15]. The use of battery as energy storage is most commonly seen and tested where excess energy is stored. However, using batteries can increase system complexity, maintenance requirements, the number of energy conversions and overall capital cost, as investigated by [16]. The cost of batteries between 2020 and 2025 is projected to be approximately \$100 to \$175/kWh, with the possibility of falling below \$75/kWh only by 2030 [17]. Additionally, batteries often have a shorter lifespan when subjected to high temperatures and frequent charge-discharge cycles [18], which is highly disadvantageous in hot climate regions.

The approach of utilising wind turbines to mechanically and directly drive the RO system was demonstrated by [12,13]. Several research projects have operated systems of such configuration by mechanically connecting the wind turbine and the pump shaft to drive water directly into the RO unit [19–24]. Additionally, vertical axis wind turbines (VAWTs) have proven to be effective in directly driving water pumps for operating RO units [13,25]. This configuration eliminates the need for complex electrical architecture, like one existed in battery-system [15].

However, the majority of these studies have shown that operating without energy storage often results in higher water costs and lower membrane efficiency due to irregular and fluctuating system operating conditions [22,26–32].

Addressing the energy intermittency issue for water desalination aimed for remote communities is crucial. The goal of this study is to investigate the feasibility and techno-economic viability of utilising VAWTs mechanically coupled to a compressed air energy system to drive an RO system; further contributing to the progress in this field. VAWTs can be sub-divided into two types: drag or lift type [33]. VAWT has attracted much attention due to its advantages over horizontal axis wind turbine (HAWT) [34]. This includes the ability to operate independently of the wind direction and eliminating the need for a yaw mechanism [33,35]. The ground-mounted drivetrain system also makes it easy for maintenance [33,35] and connection with the compressed air system and the RO unit.

The proposed configuration in this paper relies on mechanical energy to drive the compressed air energy system (CAES). Fig. 1. illustrates the proposed configuration by comparing it to a conventional configuration that uses electrical system to power the desalination unit.

Utilising CAES for energy storage may reduce complexity and cost compared to batteries in certain applications, research has shown that renewable energy-powered RO systems operating without batteries may experience lower efficiency and intermittent operation due to the fluctuating nature of renewable energy sources [26–31]. On a comparative basis, both systems address the energy intermittency issue and suitable for remote off-grid locations, but CAES appears to have a more favourable maintenance regime.

In the context of RO, various type of energy recover device (ERD) has been conceptualised and tested to recover waste energy from the rejected brine [30]. The earliest form of ERD is a simple Pelton turbine connected to a pump [30]. Subsequently, various commercial entities developed work-exchangers to recover the pressure, thus enhancing energy efficiency. These ERD devices include centrifugal, rotor and plunger types [36]. The pressure exchanger (PX), a rotary type, has been extensively used in commercial RO systems [36]. A PX ERD tested in a laboratory setting achieved an energy consumption of 3.03 kWh/m³ [36]. The implemented of ERDs in RO seawater desalination has effectively reduced the operating cost.

The points mentioned above outline the primary motivation of this research paper, which aims to develop a sustainable, less complex, low-maintenance, stand-alone system suitable for remote communities. This system uses VAWTs to directly drive CAES for operating an RO desalination plant without the need for electrical generators and batteries. The objectives are outlined as follows:

- Develop a MATLAB/SIMULINK model that represents the physical interactions between the VAWT, CAES and RO desalination unit.
- 2. Demonstrate and evaluate the model's dynamic response and robustness to varying input conditions.
- 3. Evaluate the feasibility of using CAES as an alternative to batteries.
- Investigate the impact of changes in the number of VAWTs, the presence of an energy recovery device, and other factors to determine the optimal configuration.
- Compute and compare the levelised cost of water (LCOW), initial capital costs, and maintenance expenses for different configurations at the chosen site.

#### 2. Methods

# 2.1. System and simulation model description

The system can be categorised into three main components: the wind turbine subsystem, the compressed air subsystem, and the RO desalination subsystem. In general, VAWTs utilise wind energy to generate torque, which mechanically drives an air compressor. This compressor

fills the compressed air storage, which then drives a high-pressure airoperated pump that drives the feed water (seawater) into the RO units to produce fresh water. Fig. 2 demonstrates the schematic diagram of the proposed system and shows one of the studied configurations.

The MATLAB/Simulink software was used to simulate the performance of the entire novel system. This simulation aids in understanding the system's performance, input parameters, and sensitivity analysis, ultimately leading to design optimisation and technical and economic assessment. The flow chart of the Simulink model for the proposed system is shown in Fig. 3. It illustrates the inputs and outputs of each system component. The Simulink model was developed to be flexible, allowing changes to various system components, such as varying the wind data or constant wind speed, and operating with or without the pressure exchanger.

The first input to the model is the hourly wind data for the selected location. The second input is the power curve of the wind turbine, including its parameters. The third input is the water characteristics. The following subsections detail each component of the system concerning the model equations, selections, and constraints.

#### 2.2. Wind turbine system

The wind energy block consists of the wind profile, wind turbine, and transmission. The first input to the wind turbine block is the meteorological data on wind speed. While the model has the capability to run at a constant wind speed, a useful condition for investigating individual component behaviour and validating model reliability, all the results presented in this study utilised the actual wind profile of the studied location.

# 2.2.1. Wind profile

The wind data usually has hourly values, but the model can run at different time steps. To achieve this, an interpolation function was used to look up or interpolate the values between the wind data points using a linear method. The model initially runs at various time step sizes, from monthly to minute intervals, to investigate the sensitivity of the outputs. For this study, hourly wind data from a location with an average wind speed of 5 m/s was selected to evaluate the system's performance. The chosen study site is Ras Abu Rudeis, located on the coast of the Suez Gulf in Egypt. This site was selected due to its similarities with many remote coastal areas that face water scarcity and possess abundant wind resources. This strategic choice allows the study's conclusions to be applied to a broader range of sites facing similar challenges. The wind data presented in Fig. 4 were obtained from the Photovoltaic Geographical Information System (PVGIS) [37], a tool that integrates meteorological data and geographical parameters to provide accurate insights into wind patterns.

#### 2.2.2. Mathematical model of wind turbine

Another input to the model is the power curve of the wind turbine, along with its parameters. The outputs of the wind turbine block are the

torque and revolutions per minute (RPM). The generated torque can be calculated as follows:

$$T = \frac{1}{2} \rho V_{\infty}^2 A R C_T$$
 (2.1)

where  $\rho$  is the air density,  $V_{\infty}$  is the freestream wind speed, A is the swept area (height\*2R), R is the turbine radius, and  $C_T$  is the torque coefficient.

As the wind turbine power curve is known, the torque coefficient can be found at different tip speed ratios (TSR), which represents the ratio between the tangential velocity of the turbine blade and the freestream wind velocity. The TSR can be defined as follows [38]:

$$TSR = \frac{\omega R}{V_{\infty}} = \frac{C_p}{C_{\rm T}}$$
 (2.2)

The rotational speed  $(\omega)$  can be determined using Eq. (2.2), given that the turbine radius and wind speed are known, along with the corresponding tip speed ratio (TSR) for each operating wind speed. The torque required to operate the air compressor determines the specific TSR value at a given wind speed. This dynamic adjustment of the TSR is essential for maintaining a balance between the energy capture and the energy demand of the air compressor process.

The wind turbine rotor is connected directly to the air compressor via a transmission system. To determine the specific operating point at a given wind speed, the load matching principle is applied. The rotational acceleration ( $\dot{\omega}$ ) of the rotor-compressor shaft results from the imbalance between the turbine torque ( $T_{rotor}$ ) and the resisting torque ( $T_{comp}$ ) from the air compressor. This balances the torque between the rotor and the air compressor, thus determining the turbine's rotational speed to meet the required energy to drive the air compressor. Eq. (2.3) describes the relationship between the rotor torque and the air compressor torque, with J representing the mass moments of inertia for both the rotor and the air compressor. This methodology aligns with established approaches found in the literature [19,25,39].

$$J\frac{d\omega}{dt} = T_{rotor} - T_{comp} \tag{2.3}$$

Therefore, the torque and rotational speed of the wind turbine are obtained from the wind profile, wind turbine parameters and power curves

# 2.2.3. Selection of VAWT

In this study, the power curve of the selected H-type VAWT, as shown in Fig. 5, was derived from experimental data [40,41]. In the experiment, the turbine had a swept area of  $1.5~\rm m^2$ . However, for this application, the turbine was scaled up to provide the required torque, particularly when utilising a transmission, to meet the load requirements across various wind speeds. Table 1 presents the specifications of the scaled VAWT selected for this study.

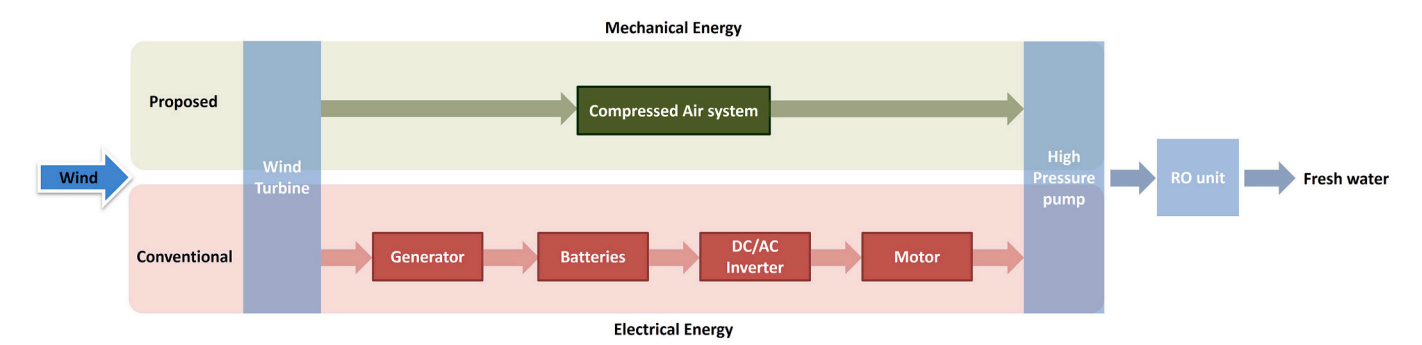


Fig. 1. A layout of the proposed system compared to a conventional system.

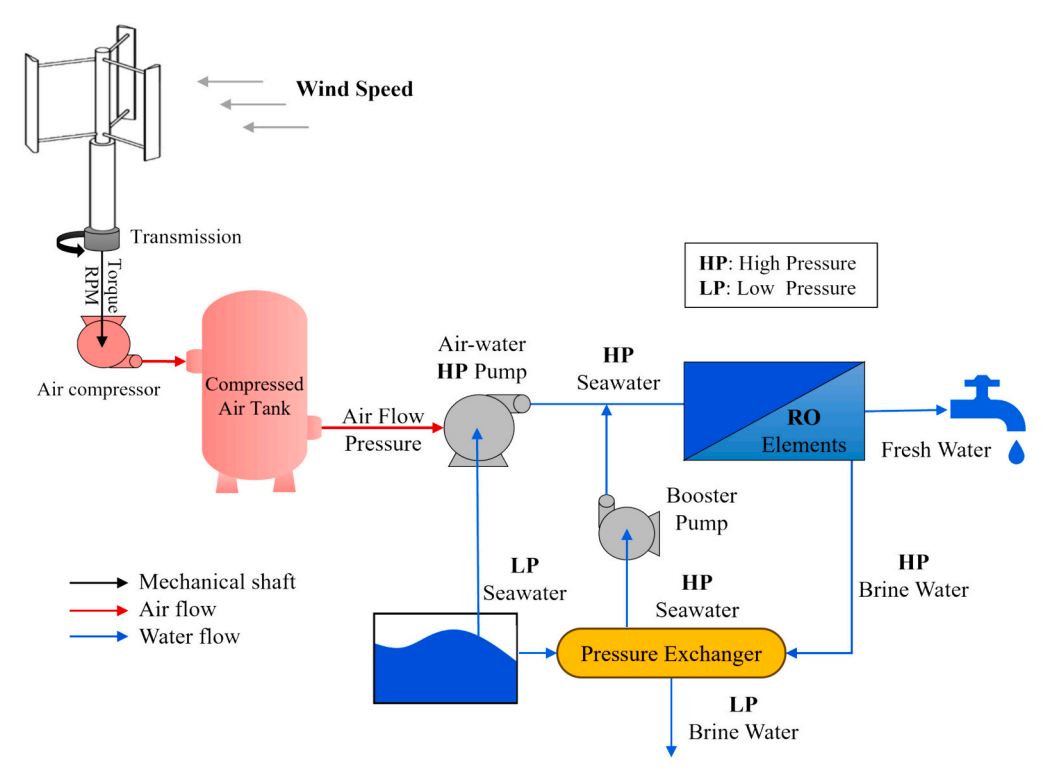


Fig. 2. A schematic diagram of the proposed, VAWT-driven compressed air energy system.

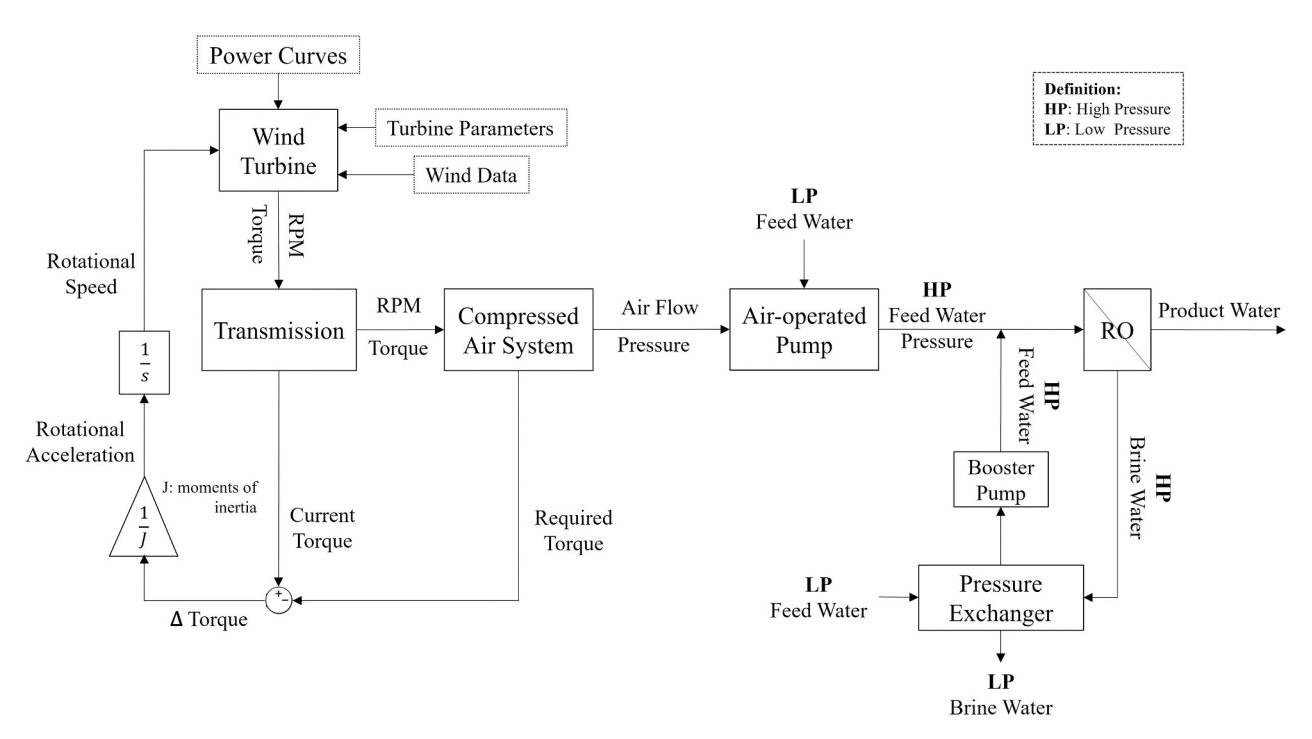


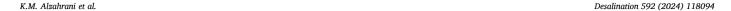
Fig. 3. Process diagram of the Simulink model for wind turbine driven CAS-RO system with pressure exchanger.

#### 2.3. Compressed air energy System (CAES)

The modelling of the compressed air energy system (CAES) is divided into two parts: air compressor, and compressed air tank. Because the output shaft of the VAWT is aligned with the vertical axis, the installation and maintenance of the CAES can be easily performed at ground level [13,25]. This accessibility contrasts with HAWT, where such processes typically involve more complexity and difficulty.

A typical small-scale VAWT operates at lower RPMs, which are generally well below the operational speed required for air compressors [42]. Therefore, a transmission is needed to match the desirable range between the VAWT shaft and the air compressor. In addition, the mechanical efficiency of the transmission was assumed to be approximately 90 %, and these losses applied to the torque generation but not the rotational speed of the turbine shaft [22].

The selection of the air compressor is limited by the torque generated



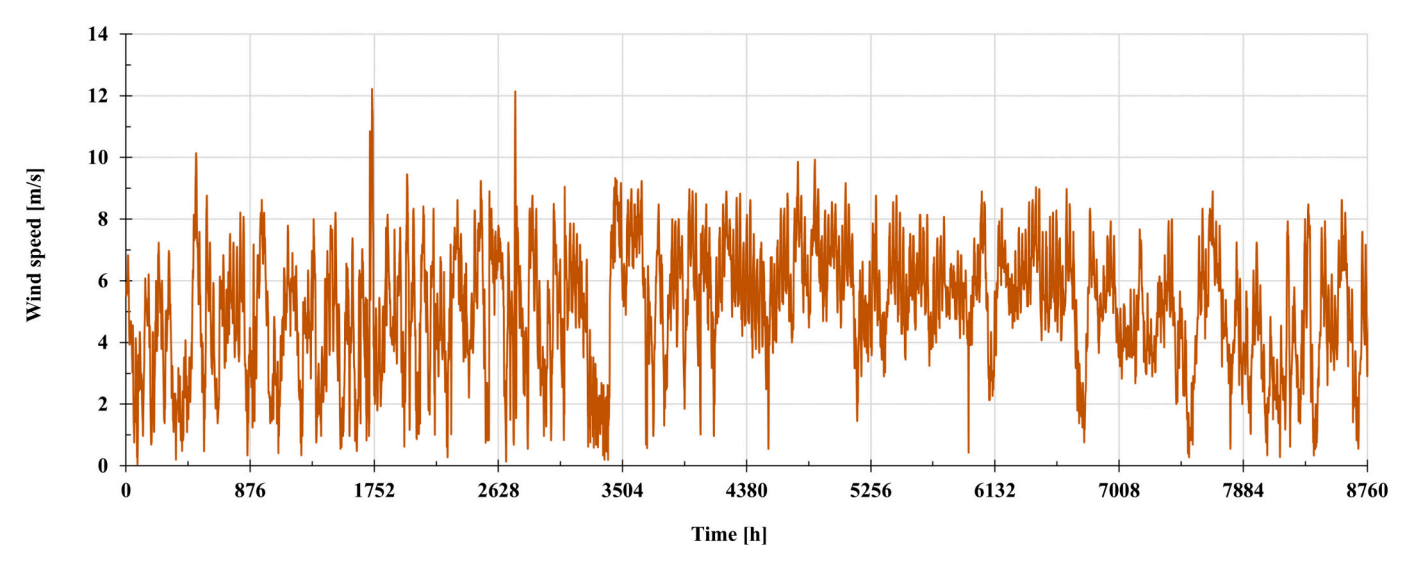


Fig. 4. The wind profile of the case study.

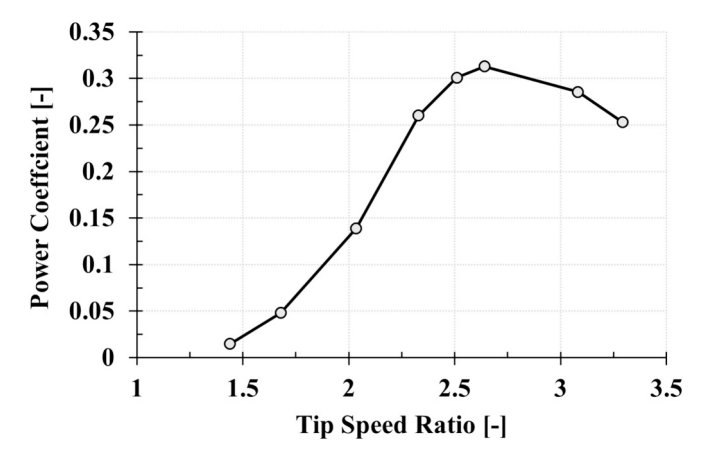


Fig. 5. The power curve of the selected VAWT [40].

**Table 1** Summary of the specifications of the selected VAWT.

Name (unit)	
Hub height (m)	5.06
Rotor diameter (m)	2.50
Swept area (m <sup>2</sup> )	12.66
Number of blades	3
Chord (m)	0.2085

by the VAWT. In this study, the air compressor was designed to operate within the torque limitations of the VAWT at the average wind speed of the study site. Therefore, it is recommended to design or modify an off-the-shelf compressor with power requirements that do not exceed the maximum power output of the VAWT.

# 2.3.1. Air compressor model

The reciprocating piston compressor, a common type of positive displacement compressor, was selected for coupling with each VAWT. The mathematical equations for modelling a reciprocating air compressor rely on the ideal gas laws and polytropic compression to provide a reliable displaced air volume at a desirable air pressure. The output of the air compressor model was validated with a commercial off-the-shelf air compressor [43]. The desired output of the air compressor model is the air flow rate at the operating pressure. Moreover, it is

important to monitor the required power and torque of the air compressor to ensure it operates below the generated power by the VAWT. The air flow rate of the air compressor (m<sup>3</sup>/s) is defined as follows:

$$Q_{air} = \frac{V_a N_{RPM}}{60} \frac{P_1 T_2}{P_2 T_1} \tag{2.4}$$

Where  $P_1$ ,  $T_1$ ,  $P_2$ , and  $T_2$  are the inlet and outlet pressures and temperatures, respectively.  $N_{RPM}$  is the speed of the compressor in revolutions per minute and  $V_a$  is the induced volume and sometimes refers to the free air delivery per stroke, which is given by:

$$V_a = \eta_{\nu} V_s \tag{2.5}$$

$$\eta_{\nu} = 1 + C - C \left( \frac{P_2}{P_1} \right)^{\frac{1}{n}} \tag{2.6}$$

$$V_s = \frac{\pi}{4}D^2L \tag{2.7}$$

Where  $\eta_{\nu}$  is the volumetric efficiency after neglecting the leakages. C is the clearance ratio between the clearance volume and the swept volume (Vs). D and L are the cylinder bore and the length of the stroke, respectively. The clearance volume is assumed to be 15 % of the swept volume, and the polytropic exponent (n) is 1.25 [44]. The indicated power and the required power of the air compressor are defined as follows:

$$\textit{Indicated Power}(\textit{IP}) = \frac{V_a \ N_{\textit{RPM}}}{60} \times \frac{n}{n-1} \ P_1 \left[ \left( \frac{P_2}{P_1} \right)^{\frac{n-1}{n}} - 1 \ \right] \tag{2.8}$$

Required Power = 
$$\frac{IP}{\eta_m}$$
 (2.9)

Where  $\eta_m$  is the mechanical efficiency, and it is approximated to be 95 % [44]. Eventually, the required torque can be obtained by using the following equation.

$$T = \frac{P}{\omega} \tag{2.10}$$

# 2.3.2. Compressed air tank model

The second component of the CAES is the compressed air tank, which is a pressure vessel for air storage. The size of the tank is an important parameter and is determined based on the desirable operating time of the system, the maximum duty cycle, and the water demand aimed at

the target communities. In this research, a 2000-L compressed air tank was chosen with a maximum pressure capacity of 11.5 bar [45], equivalent to 23,000 L of uncompressed air.

When designing the air storage, the minimum and maximum pressures, operation pressure, and outlet flow rate of the compressor need to be considered. In the case where the operating pressure is below the minimum level, the tank outlet closes so the system can operate at constant pressure and outlet flow rates. The tank capacity was modelled using Boyle's law and mass balance as follows:

$$P_a V_a = P_c V_c \tag{2.11}$$

$$V_c = \frac{t \, Q_G \, P_a}{(P_{\text{max}} - P_{\text{min}})} \tag{2.12}$$

Where  $P_aV_a$  are the pressure and volume of a gas at atmospheric pressure, and  $P_cV_c$  are the pressure and volume of a gas after compression, respectively. t is the time for the tank to raise the minimum tank pressure  $(P_{min})$  to the maximum tank pressure  $(P_{max})$ .  $Q_G$  is the outlet delivery gas flow rate at a specific regulating pressure. Therefore, in the Simulink model of the air tank, the flow rate from the air compressor is integrated to accumulate the tank pressure with consideration of the tank maximum limit. Monitoring the tank's pressure is important to determine when to close or open the outlet valve to operate the air-operated HP pump.

#### 2.4. Air-operated high-pressure pump

As shown in Fig. 3, the outlet of the compressed air energy system is the inlet of the air-operated HP pump with the assistance of a control value to have a constant operation that is suitable to operate the RO unit. The air-operated HP pump has the highest energy consumption of the system, as the RO desalination process needs pressurised feeding water between 20 and 60 bars [46], mainly depending on the salinity of the feeding water. Most HP pumps in RO desalination plants are powered by electricity; however, in this proposal investigation, the HP pump is driven by compressed air, which comes directly from the compressed air energy system.

## 2.4.1. Air-operated HP pump selection and modelling

The selected air-operated HP pump has a pressure ratio of 1:7 and it is a double-acting pump. The range of the inlet air pressure is from 2.1 to 8.3 bar, and the range of the outlet water pressure is from 14.5 to 69.6. More details can be found in the manufacturers data [47]. This air-operated HP pump was utilised for all studied cases. The pump specifications are presented in the supplementary materials 8.3. The relation between the outlet water flow rate of the HP pump and inlet air

consumption is shown in Fig. 6 (a). The outlet water pressure with respect to the outlet water flow rate is shown in Fig. 6 (b) [47]. Other operating air pressures can be found in the supplementary materials S.3. In the Simulink model, an interpolation function was used to simulate the output of the HP pump.

#### 2.5. RO desalination unit

The greater the number of RO membranes connected in series or parallel, the higher is the recovery ratio that can be obtained. However, in small-scale stand-alone plants, there is a limitation due to the high pressure and flow rate requirements for having more RO membrane elements in series, pressure vessels in parallel, and stages. In the literature, about 1-6 membranes are usually used for small-scale stand-alone plants for sea or brackish water, as shown in the research projects [20,22,27,48-50]. Typically, in seawater desalination, the system has single-stage systems due to the high salinity [46], as the product water of a second stage will usually have high total dissolved solids (TDS), which could be above the standard TDS in drinking water. Adding the average individual recovery rate per membrane, it varies between 7 and 12 % [46]. Therefore, in this study, a single stage with two membranes in a single pressure vessel was selected. Also, the Simulink model has the flexibility to change the RO configurations to conduct the technical assessment

The type of feeding water from brackish to seawater can easily change the design, limitations, and operating range of the RO process. This study focuses on desalinating seawater, specifically at the Red Sea location where the study site is located, with a total TDS concentration of approximately 42,200 mg/L [51], higher than the standard seawater composition (35,000 mg/L) [46].

#### 2.5.1. Modelling and simulation

The modelling of the RO process was based on the solution-diffusion model, Darcy's law, mass balance, and empirical equations, as presented in the following references [46,52–56]. The rate at which permeate flows across the membrane depends on the difference between feed pressure and osmotic pressure, and this can be approximated using the following equation:

$$Q_{p} = A_{\text{perm}} S_{e}(\text{TCF})(\text{FF}) \left[ \left( P_{f} - \frac{\Delta P_{fc}}{2} - P_{p} \right) - \left( \pi_{fc} - \pi_{p} \right) \right]$$
 (2.13)

Where  $Q_p$  (m³/h) represents the permeate flow rate and  $A_{perm}$  denotes the membrane permeability (m³/(m²-h-bar)). The membrane surface area  $S_e$  (m²) is defined in Table 2. Eq. (2.13) states that permeate flow rate is directly proportional to the net driving pressure. This means that

80

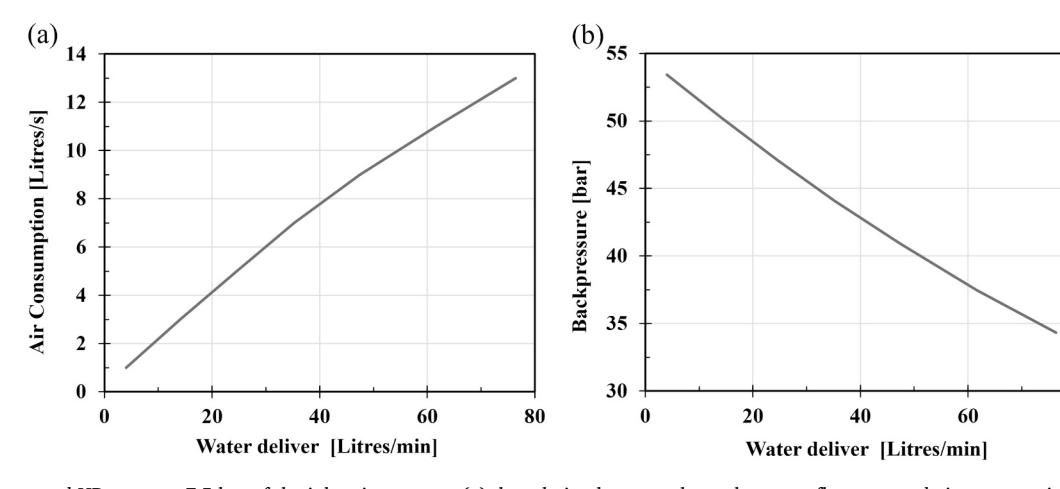


Fig. 6. The air-operated HP pump at 7.5 bar of the inlet air pressure, (a) the relation between the outlet water flow rate and air consumption. (b) the outlet water pressure versus the outlet water flow rate (adapted from [47]).

higher feed pressure and lower solute concentration in the feed water result in a faster flow of permeate through the membrane.

In the RO process, an increase in the feed water temperature leads to a higher permeate flow rate. To account for this, a temperature correction factor (TCF) is incorporated into the equation, estimated using formulas provided by the membrane manufacturer [46]:

$$TCF = \left\{ \begin{array}{c} exp \left[ 2640 \left( \frac{1}{198} - \frac{1}{273 + T} \right) \right], T \geq 25^{\circ}C \\ exp \left[ 3020 \left( \frac{1}{198} - \frac{1}{273 + T} \right) \right], T < 25^{\circ}C \end{array} \right\}$$
 (2.14)

Where T (°C) represents the feed water temperature. FF denotes the membrane fouling factor, which assumes a value of unity for a new membrane.  $P_f$  (bar) stands for the feed water pressure, and  $P_p$  for the permeate pressure.  $\Delta P_{fc}$  is the pressure drop on the concentrate-side, and it is estimated by the following empirical formula:

$$\Delta P_{fc} = 0.756 \left( \frac{Q_c + Q_f}{2} \right)^{1.7} \tag{2.15}$$

Where  $Q_c$  is the concentrate flow rate and  $Q_f$  is the feed flow rate. The  $\pi_{fc}$  is the average concentrate-side osmotic pressure, determined as follows:

$$\pi_{fc} = \pi_f \left(\frac{C_{fc}}{C_f}\right) \text{CPF}$$
 (2.16)

 $C_{fc}$  (mg/L) is the average feed concentration on the concentrate side of the membrane, and this is calculated using Eq. (2.17), which accounts for the water recovery ratio (Y), the ratio of the permeate flow to feed flow.  $C_f$  is the feed concentration in the feed water. CPF is the concentration polarisation factor, which accounts for the increased concentration of solutes near the membrane surface compared to the bulk solution. This is calculated using Eq. (2.18).

$$C_{\rm fc} = C_f \ln \left(\frac{1}{1-Y}\right)/Y \tag{2.17}$$

$$CPF = e^{0.7Y} \tag{2.18}$$

Therefore, Eq. (2.16) estimates the osmotic pressure on the concentrate side of the membrane by adjusting the feed osmotic pressure based on the concentration changes and polarisation effects occurring during the RO process. The osmotic pressure at given temperatures and salinities can be found as follows:

$$\pi_i = \left\{ \begin{array}{c} \frac{C_i \ (T+320)}{491000}, C_i < 20000 \ \text{mg/l} \\ \frac{0.0117 \ C_i - 34}{14.23} \frac{(T+320)}{345}, C_i > 20000 \ \text{mg/l} \end{array} \right\} \text{ bars } \quad (2.19)$$

In Eq. (2.13),  $\pi_P$  represents the osmotic pressure of the permeate, which can be calculated as:

$$\pi_p = \pi_f(1 - R) \tag{2.20}$$

**Table 2**The detailed specification of each selected membranes for the studied cases.

Name (unit)	RO membranes		
_	SW30-4040 [63]	SW30XLE-400 [64]	
Active area, S (m <sup>2</sup> )	7.30	37.00	
Membrane length, L (m)	1.02	1.02	
Membrane diameter, D (m)	0.10	0.20	
Maximum feed flow rate (m <sup>3</sup> /h)	3.60	14.10	
Minimum feed flow rate (m <sup>3</sup> /h)	0.91	3.41	
Minimum salt rejections (%)	99.50	99.60	
Maximum element recovery (%)	13	13	
Membrane type	Polyamide thin-film composite		

where  $\pi_f$  is the osmotic pressure of the feed water and R is the salt rejection of the membrane element, a value typically provided in the manufacturer's datasheet.

So far, with the assistance of the above equations, the permeate flow rate can be determined using Eq. (2.13). Subsequently, the permeate concentration  $(C_n)$  can be calculated using the following equation:

$$C_p = B_{\text{salt}} S_e(\text{TCF}) \left[ \text{CPF} \left( \frac{C_{fc}}{Q_p} \right) \right]$$
 (2.21)

Where  $B_{salt}$  is the salt permeability of the membrane. The values of both  $B_{salt}$  and  $A_{perm}$  (water permeability) depend on the flow rate, surface area, and feed pressure, varying across different types of RO membranes and operating conditions. Therefore, these values were obtained from the membrane manufacturer's datasheet for each specific case. The manufacturer also provides software called WAVE, designed to assist in optimising RO system design and determining the ideal operating conditions and membrane types for specific applications [57].

Assuming incompressible flow, the concentrate flow rate  $(Q_c)$  and its concentration  $(C_c)$  were determined using the mass balance equations:

$$Q_f = Q_p + Q_c \tag{2.22}$$

$$C_f Q_f = C_p Q_p + C_c Q_c \tag{2.23}$$

For systems utilising multiple membranes, as in this study, Eq. (2.22) and (2.23) can be employed to calculate the total flow rates and concentrations. Two different types of RO membranes were utilised in this work, due to the various configurations investigated, which resulted in different operating ranges of water flow rates. Table 2 presents the main characteristics and operating ranges of the two selected RO membranes.

# 2.6. Pressure exchanger (PX)

The pressure exchanger (PX) was used as an energy recovery device (ERD) to recover the energy losses from the concentrated water (brine). In this study, the PX was only utilised in configurations with high flow rates due to the minimum flow rate requirement of the smallest commercially available PX. Furthermore, as the selected air-operated HP pump is a fixed size for all cases, the inclusion of the PX contributes to increasing the feed water flow rate to the RO unit. This adjustment requires changing the type of RO membrane to accommodate the new flow rate, as shown in Table 2. The selected pressure exchanger is from the Energy Recovery Company and the PX30 is the smallest PX that can be used with an operation range of the flow rate from 4.5 to 6.8 m<sup>3</sup>/h [58]. The minimum guaranteed efficiency of the PX30 is about 93.4 % at 5.6 m<sup>3</sup>/h [59]. The PX specifications and general information are presented in the supplementary materials S.5.

A mass balance model was applied to simulate the flow inlets and outlets of the PX. Within the PX, salinity mixing occurs as the feed water interacts with the brine water. This interaction leads to an increase in the salinity levels of the feed water. However, the PX mixing ratio in the PX is considered to be very small, <3% [60] if the system runs in the operational range. Therefore, for simplicity, the mixing ratio is neglected in the modelling. In this case, the high-pressure water leaving the PX has a flow rate and pressure similar to the concentrated high-pressure water entering the PX multiplied by the PX efficiency.

Software from the same manufacturer as the PX, called the Power Model Pro [61], is designed to simulate the PX performance with an RO system. It can assist in the PX selection to find the optimum option and the economy and energy aspects. In this study, the Power Model Pro software was used to validate the outcomes of the studied cases using the Simulink model.

The high-pressure water of the PX outlet is also pumped by a circulating booster pump and enters the RO membrane unit, as shown in Fig. 3. Given that a compressed air energy system operates the system,

the selected booster pump needs to operate with the same technology that is much like the high-pressure pump. Moreover, the energy consumption by the circulating pump is almost negligible compared to the HP pump since the booster pump mainly circulates and maintains the pressure but does not pressurise the water. Approximately, the air consumption of the air-operated LP pump is between 4 and 8 m $^3$ /h [62] at 5 bar, but these values depend on the selected cases.

#### 2.7. Techno-economic assessment

Each component of the system was modelled in the MATLAB/ Simulink to simulate its performance and make it adaptable for evaluating its technical and economic feasibility. The system model can simulate the water production from the provided wind data for the studied location.

# 2.7.1. Selection of the parametric cases

The primary differences among the studied configurations are the number of VAWTs and the inclusion of a pressure exchanger (PX). A total of 28 configurations were analysed. The first 15 configurations, operating with 1 to 15 VAWTs, do not include a PX. The remaining 13 configurations incorporate a PX, with the number of VAWTs ranging from 3 to 15. The performance impact of the PX is visible in configurations 16–28, which can be compared with configurations 3–15 that have a similar number of VAWTs but lack a pressure exchanger. All cases utilise the same wind profile, as shown in Fig. 4.

Changing between these configurations results in changes in the flow rate of the feed water, which affects the performance of the RO membranes. For this reason, changing the type of RO membranes is necessary to have an optimum recovery ratio. The WAVE, the RO system simulator, from the membranes manufacturer was used to assist in finding the optimum type of membranes for the studied cases [57]. Two types of RO membranes have been found, as listed in Table 2, that are able to cover the range of the feed water flow rate of all studied configurations [46].

# 2.7.2. Levelised cost of the water calculation

The cost of the water production depends mainly on the cost of the VAWT, compressed air energy system, high-pressure pump, and RO units. Operation and maintenance costs, economic lifetime, recovery factor, and discount rate were also taken into account to evaluate the cost over time. The lifetime of the system is 25 years, and the discount rate is 8 % [65]. Table 3 shows the unit price of the system components. Since the turbine was selected based on the experimental data, its price was compared to available market options. However, no turbine of the same size was found. Therefore, various sizes of VAWTs, along with their swept areas and prices, were listed to approximate the cost for the selected VAWT size. Curve fitting was then employed to estimate the cost for the corresponding swept area. Details of the listed prices and curve fitting can be found in the supplementary materials S.2.

The total annual operation and maintenance (O&M) cost is the sum of these three costs: annual labour cost, chemical cost, and replacement cost. The annual labour cost is defined as the annual production (in  $m^3$ )

**Table 3**The cost of the system components is per unit price.

Name	Unit price [US\$]	Ref.
VAWTs	6488	[66,67]
Air compressor	174	[68]
Compressed air tank	3510	[45]
high-pressure pump	11,371	[69,70]
Booster pump	730	[71]
RO membrane SW30-4040	500	[72]
RO membrane SW30XLE-400	830	[73]
Pressure exchanger	7600	[58,74]
Pre- and post-treatment	12 % of total RO plant capital cost	[53]

multiplied by the specific operating labour cost  $0.05~\text{US}\slash\text{m}^3$ . Likewise, the annual chemical cost is about  $0.033~\text{US}\slash\text{m}^3$ , which includes pre-and post-treatment and depends on the water condition. Moreover, the installation and infrastructure costs were considered to be 30 % of the capital cost of the system [65,75].

The annual replacement cost is the sum of each component's cost multiplied by its replacement rate. Such as the RO membrane, which is often replaced every three years, but the pumps have longer lifespans. These values can be found in the datasheet for the system parts. Therefore, after calculating the O&M cost and capital cost for each case, the levelised cost of water (LCOW) can be obtained as follows:

$$LCOW = \frac{Capital\ Cost \times CRF + O\&M\ Cost}{Annual\ Water\ Production} \left[ US\$/m^3 \right]$$
 (2.24)

Where the CRF is the capital recovery factor, it can be determined as follows:

$$CRF = \frac{(1+r)^n r}{(1+r)^n - 1} \tag{2.25}$$

And n is the system lifetime, and r is the discount rate.

# 3. Results and discussion

The techno-economic assessment was conducted using system component models and the cost calculations detailed in the previous section, along with the component prices listed in Table 3. A total of 28 different configurations were implemented in the Simulink model to evaluate system performance. These configurations were chosen to illustrate the impact of varying system parameters, such as the number of VAWTs and the inclusion of a pressure exchanger (PX), on the levelised cost of water (LCOW), annual water production (AWP), and capital cost.

A solution-independent numerical study of the time-step size was conducted to determine the optimal balance between accuracy and computational cost in the simulated model. The model was run using various time-step sizes to identify a value at which model results become insensitive to further changes. An hourly time step size was selected for the system performance simulation, as it offered the lowest computational cost while maintaining acceptable accuracy in representing the model.

# 3.1. VAWT performance and monthly water production

The selected VAWT was implemented in the system model to investigate its performance in terms of torque generation, rotational speed, annual water production (AWP), and levelised cost of water (LCOW). When coupled with an air compressor, the wind turbine's operation differs depending on the connection type. In a mechanical connection, the operating point (or optimum TSR) is determined by the equilibrium between the turbine's torque generation and the air compressor's load demand, as explained in Section 2.2.2.

Fig. 7 demonstrates the performance characteristics of the wind turbine directly coupled with the air compressor. The figure plots the power (W) and torque (Nm) against wind speed (m/s). Each point in the figure represents an hour of the selected wind profile over the course of a year, providing a comprehensive view of the system's performance under varying wind conditions. The power curve (black circles) shows a smooth increase in power output as the wind speed increases, starting from around 4 m/s. The almost linear increase in power with wind speed is essential for maintaining a consistent torque to operate the air compressor, as governed by Eq. (2.10). This linearity ensures the turbine's output matches the torque demand of the air compressor, thus enabling efficient operation.

The torque curve (orange squares) in Fig. 7 initially rises with increasing wind speed, indicating that the turbine needs to generate

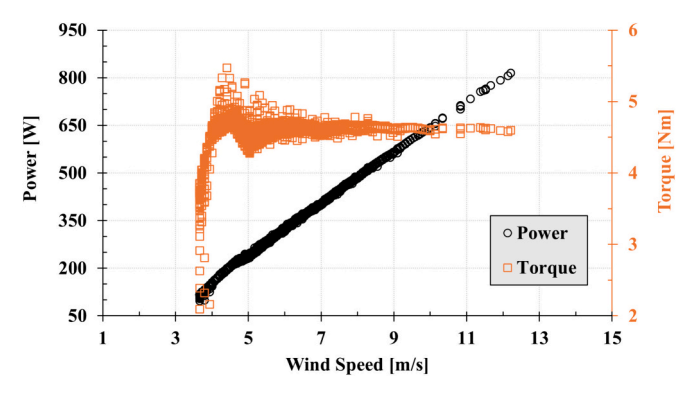


**Fig. 7.** Hourly values from the selected wind profile over a year illustrate the performance characteristics of the wind turbine coupled with the air compressor.

more torque to drive the air compressor. This trend continues until around 5 m/s, after which the torque plateaus. This levelling off occurs as the turbine adjusts its rotational speed to maintain the required torque for the air compressor, ensuring an optimal balance between energy capture and energy demand. The overshoot in the torque curve can be attributed to the moments of inertia of the turbine. Turbines with lower inertia tend to experience more overshoots in torque generation during rapid increases in wind speed, while higher inertia can lead to torque overshoot during decreasing wind speeds, indicating that inertia plays a role in the dynamic response of the system.

The relationship between torque and power at various wind speeds illustrates the equilibrium between the turbine's mechanical output and the air compressor's demand. The turbine's ability to adjust its rotational speed to meet the air compressor's torque demand at different wind speeds highlights the dynamic nature of this equilibrium and the effectiveness of the direct mechanical coupling. This representation over a year's worth of hourly data gives a robust validation of the system's performance across a wide range of operational conditions.

Fig. 8 illustrates the monthly water production of the VAWT-CAES-RO system, which includes three VAWTs and a pressure exchanger (PX) as an energy recovery system, considered the baseline case. As shown in Fig. 4, the wind profile of the studied site indicates that the average wind speed is highest in summer. Additionally, during the summer months, a larger fraction of hourly wind speed values exceeds the cut-in speed of approximately 3.6 m/s, based on the load demand's torque requirements. Consequently, the system produces more fresh water during the summer months, with July being the peak month for water production. This baseline case achieved an annual water production of 2554 m³ with a levelised cost of water (LCOW) of 3 US\$/m³. For a comparison between all the studied cases, refer to Fig. 11.

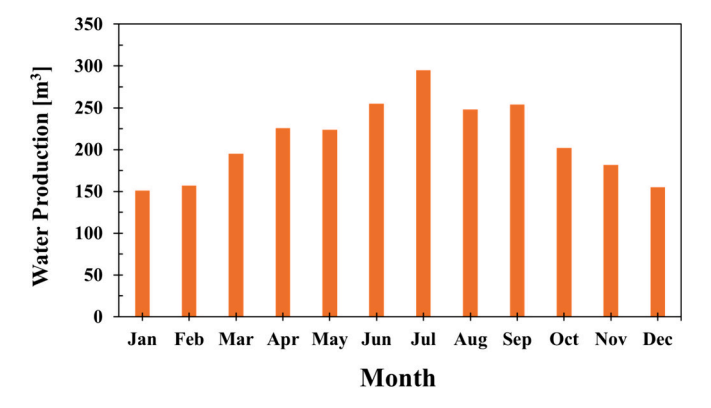


Fig. 8. Monthly water production of the VAWT-CAES-RO system using three VAWTs and a PX at the study site.

#### 3.2. Performance of VAWT-CAES-RO system

Fig. 9 provides a snapshot of the performance metrics of the VAWT-CAES-RO system, using the baseline configuration of three VAWTs and a pressure exchanger (PX), over a 48-h period. Fig. 9 (A) illustrates the relationship between wind speed, turbine torque after transmission, tip speed ratio (TSR), and the required torque for the air compressor. The torque demand of the air compressor is assumed to be constant under steady-state conditions since it generally maintains nearly constant torque across various rotational speeds and power levels (except at the initial point), which is typical for a piston displacement air compressor [44,76]. The turbine consistently provides the required torque to the air compressor as long as the wind speed remains above 3.6 m/s (the cut-in speed). This performance depends on the transmission ratio and air compressor size. The impact becomes clear around the 42-h mark when the wind speed briefly drops below 3.6 m/s, resulting in a significant decrease in turbine torque generation. This decrease is insufficient to drive the air compressor, resulting in turbine stall. The TSR curve demonstrates the turbine's ability to adjust its rotational speed to meet the torque demand. As the wind speed increases, the TSR also increases to maintain the required torque. This results in a higher airflow rate and, consequently, increased water production.

Fig. 9 (B) illustrates the operational dynamics of the compressed air energy storage (CAES) system integrated with the RO desalination process over a 48-h period. The selected compressed air tank has a capacity of 2000 L and can handle a maximum pressure of 11.5 bar. During 0 to 6 h period, the tank pressure increases rapidly from 0 bar to 11 bar as the system charges the air tank. The system operates with a pressure range of 8 to 11 bar, controlled by an on/off controller. The tank is charged until it reaches the upper limit of 11 bar, at which point the outlet valve opens to supply pressurised air to the air-operated highpressure (HP) pump, driving the RO process. The tank continues to discharge until the pressure reaches the lower limit of 8 bar, triggering the closure of the outlet valve and the resumption of charging. The frequency of charging and discharging cycles of the compressed air tank is directly influenced by the wind speed. As the wind speeds increase, the frequency of these cycles also rises, indicating a more dynamic energy storage and release process. On the other hand, when the wind turbines stop due to insufficient wind speeds, as observed around the 44h mark, the tank's pressure remains constant, stopping both charging and discharging until the wind speed picks up again.

This cyclical operation ensures that the air-operated HP pump receives a consistent supply of pressurised air at approximately 7.5 bar, which has a 1:7 air-to-water pressure ratio. As described in section 2.4.1, this 7.5 bar of pressurised air operates the air-water to pressurise feed water to around 48 bar, which is considered ideal for selected RO membrane operation. The air flow rate also fluctuates, mirroring the wind speed changes. However, there is a sharp drop-in air flow rate to zero around the 42-h mark when wind speed dips below 3.6 m/s. Additionally, the air flow rate is directly influenced by the number of operational wind turbines, which in turn depends on the current wind speed. An additional 48-h performance analysis is available in supplementary materials S.1 for further illustration of the system's behaviour.

Fig. 10 illustrates the system's performance over the first month, extending the observations made in Fig. 9 to a longer period. This provides a comprehensive view of how the system behaves over time. Particularly, the average wind speed over the first month is around 4 m/s, lower than the 5 m/s average observed in Fig. 9 for the two-day period. This lower average wind speed for the first month explains the lowest monthly water production observed in Fig. 8. This low wind speed also accounts for instances of turbine stalling and stopping the operation, as the wind speed frequently falls below the cut-in speed required to generate torque and drive the air compressor. The torque (red line) remains relatively stable around the required torque level, thanks to the turbine's ability to adjust its TSR (green line) to maintain the necessary torque for air compressor operation. The system

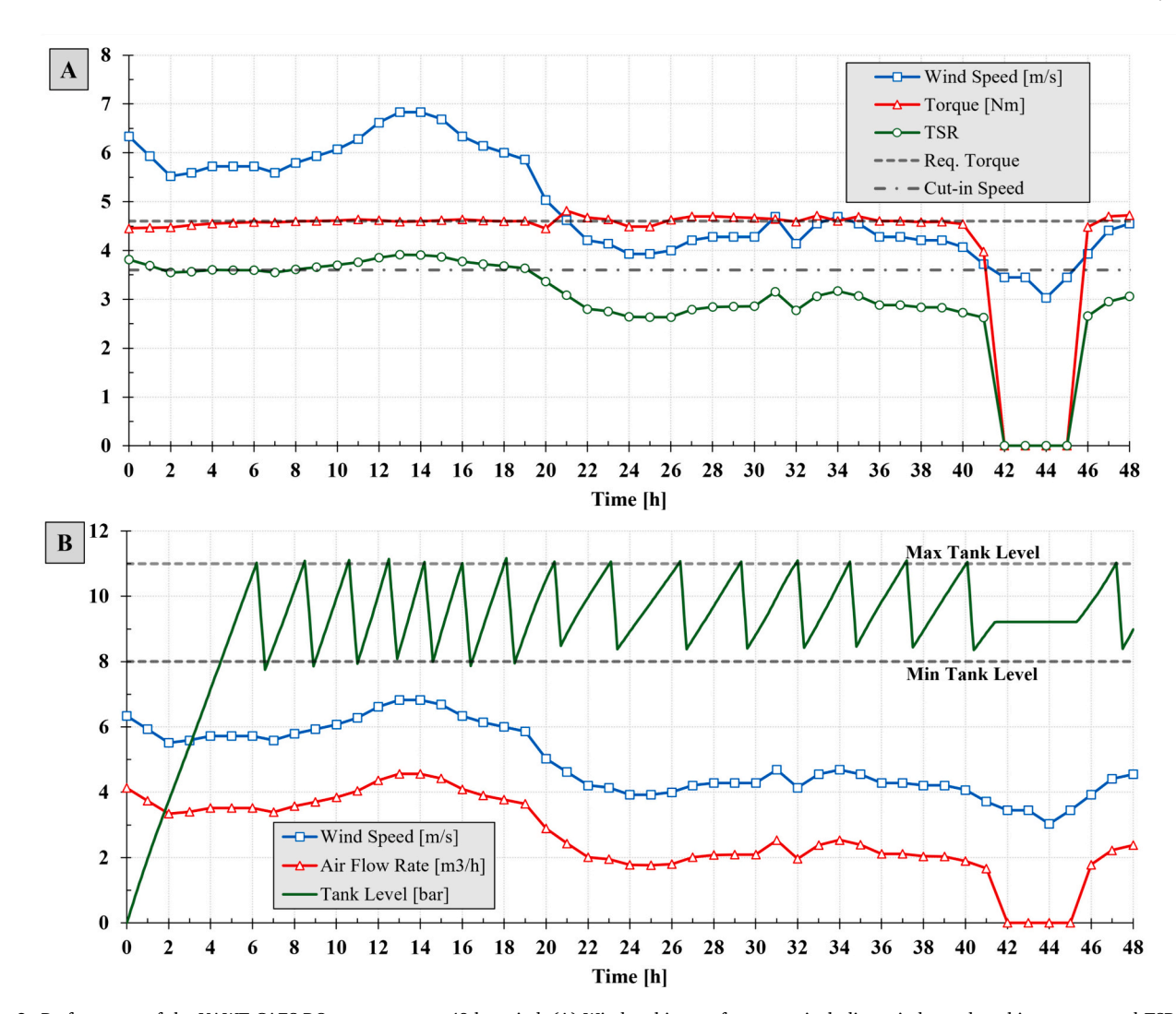


Fig. 9. Performance of the VAWT-CAES-RO system over a 48-h period: (A) Wind turbine performance, including wind speed, turbine torque, and TSR; (B) CAES performance, showing the air flow rate and tank pressure.

demonstrates stability over the month, maintaining the tank pressure within the desired range despite variable wind conditions. This ensures a consistent supply of pressurised air to the air-operated HP pump, maintaining optimal operating conditions for the RO unit. For further analysis and comparison, the supplementary materials S.1 provides data from another randomly selected month, thus offering additional insights into the system's long-term behaviour and performance under different wind conditions.

In practical applications, the efficiency of the air compressor is crucial, particularly as it operates over a wide RPM range. Variations in efficiency can affect the power required to maintain air pressure, thus impacting overall system performance. To minimise efficiency losses, it is important to select a compressor that is highly efficient across varying conditions and possibly implement advanced control strategies to optimise operation in response to changing wind speeds. This consideration is a key area for future research to improve overall system performance.

# 3.3. Results of the techno-economic assessment

The system performance presented in Figs. 8, 9 and 10 reflects the baseline configuration, which utilises three VAWTs, each directly coupled with an air compressor, along with a single pressure exchanger (PX). The corresponding levelised cost of water (LCOW) and annual water production for this configuration are shown in Fig. 11 (B), along

with other configurations. Fig. 11 illustrates the relationship between LCOW and annual water production across 28 different cases of the system, varying the number of VAWTs and the use of a PX. Fig. 11 (A) displays the first 15 configurations without a PX, while Fig. 11 (B) shows the 13 configurations that include a PX. It is important to note that the selected air-operated high-pressure (HP) pump and the capacity of the compressed air tank are fixed for all cases. Consequently, the use of the PX increases the feed water flow rate to the RO unit, ultimately reducing the LCOW.

The points in Fig. 11 indicate the number of VAWTs used in each configuration. The first 15 cases in Fig. 11 (A) do not use an energy recovery device, PX. Case 1, which utilises a single VAWT without a PX, results in the highest LCOW of approximately  $18 \text{ US} \text{ J/m}^3$  and the lowest annual water production of around  $223 \text{ m}^3$  (0.6 m³ per day). Among the cases without a PX, Case 9, with nine VAWTs, achieves the lowest LCOW of  $5.53 \text{ US} \text{ J/m}^3$ .

For the 13 cases (Cases 16–28) in Fig. 11 (B), a PX is introduced. Case 16 (baseline), which uses three VAWTs with a PX, significantly reduces the LCOW to approximately 3 US\$/m³ and increases the annual water production to around 2550 m³. As the number of VAWTs increases from 3 to 15, the LCOW gradually decreases, reaching its minimum in Case 24, which employs 11 VAWTs and achieves the lowest LCOW at 1.63 US \$/m³, with an annual water production of nearly 9400 m³. Beyond this point, the LCOW starts to increase as the system reaches the full capacity

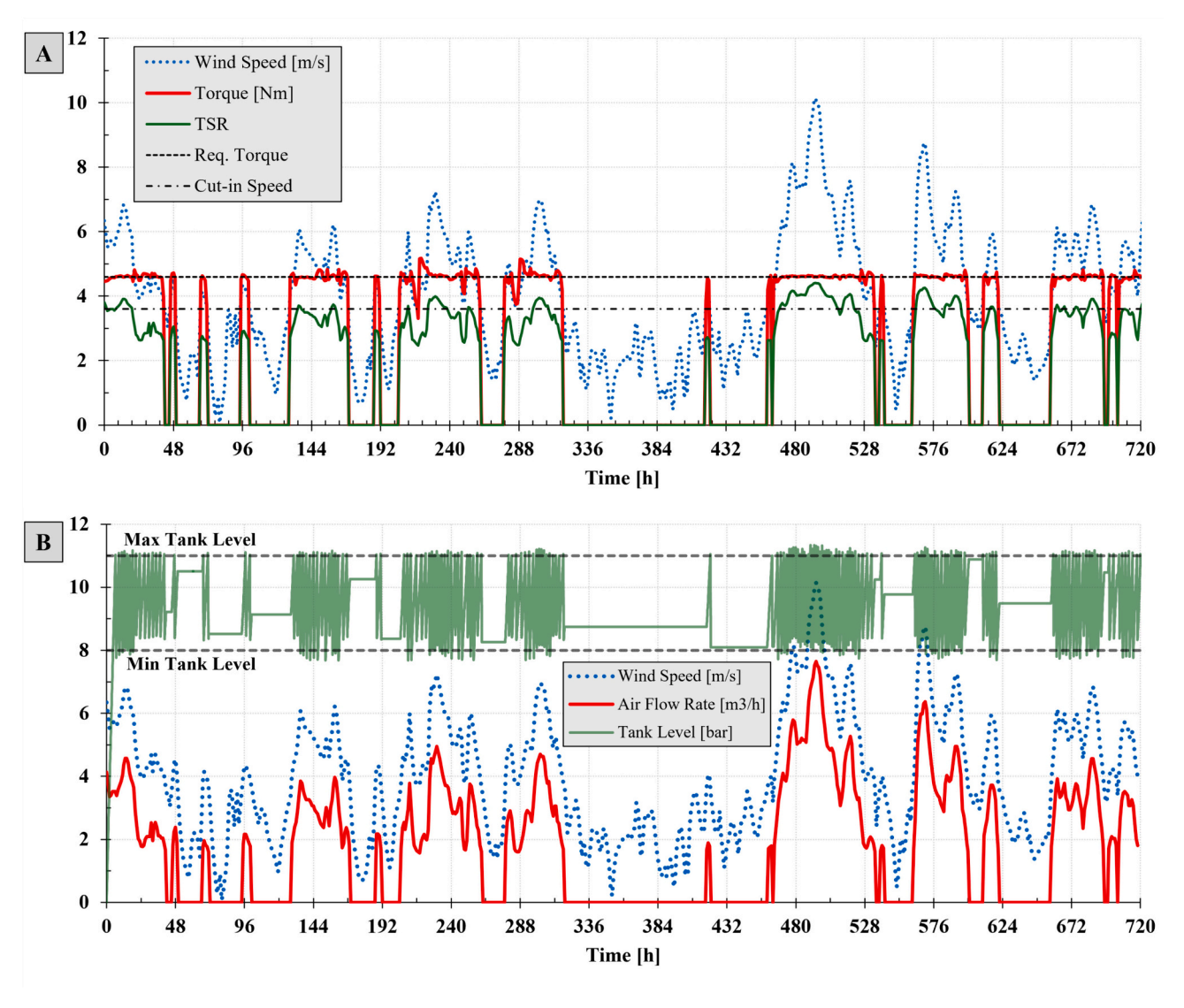


Fig. 10. Performance of the VAWT-CAES-RO system over a month: (A) Wind turbine performance, including wind speed, turbine torque, and TSR; (B) CAES performance, showing air flow rate and tank pressure.

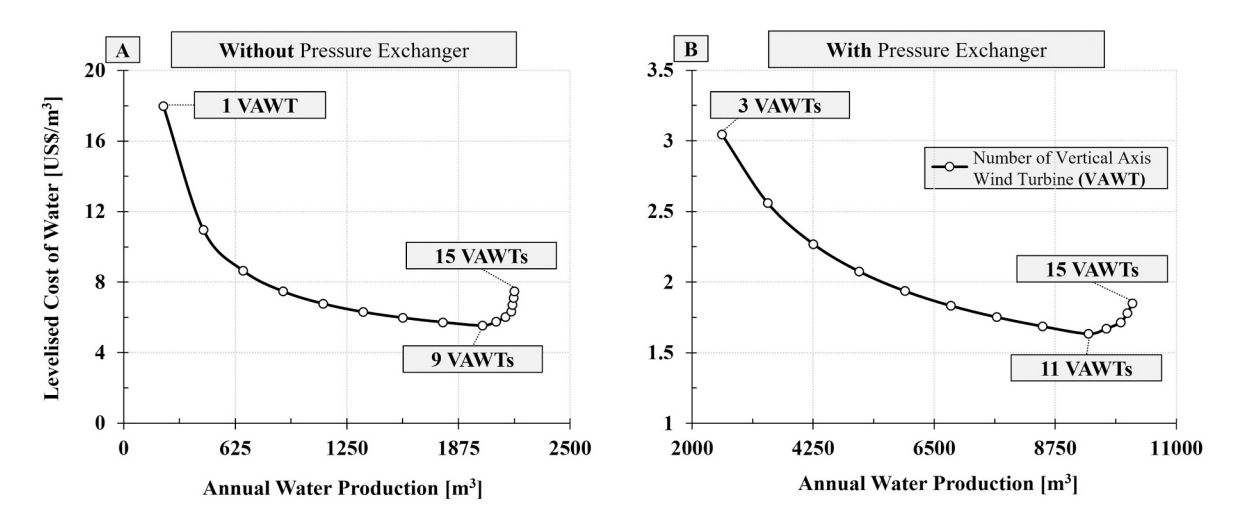


Fig. 11. Annual water production and LCOW for the 28 configurations of the VAWT-CAES-RO system, with an increasing number of VAWTs. (A) Cases without a PX, and (B) cases with PX.

of the compressed air tank, requiring venting of the excess air.

The key observations are that increasing the number of turbines significantly reduces the LCOW and increases water production. However, the lack of a PX in the first 15 cases limits efficiency gains. The introduction of the PX from Case 16 leads to a substantial reduction in LCOW and a significant increase in water production, emphasising the importance of energy recovery for enhancing system efficiency. Adding more turbines beyond the optimal point does not further reduce the LCOW significantly, indicating a saturation point.

Although the PX accounts for approximately 13 % of the capital cost of Case 16 (the baseline with 3 VAWTs), as illustrated in the cost breakdown in Fig. 12, it delivers a significant reduction in the LCOW. While the PX could theoretically be applied to configurations with 1 or 2 VAWTs, the flow rate limitations of the smallest PX available at the time of this study requires a minimum of three VAWTs to meet the PX's minimum operating point [58]. Consequently, Fig. 11 (B) begins with the case of 3 VAWTs.

The results from the Simulink model were validated using the WAVE software [57]. Cases 1 to 15 share similar conditions after the air-operated HP pump, as the airflow rate is controlled to regulate the outlet of the compressed air tank. Consequently, the only variation among these cases is the percentage of operation, which increases with the number of turbines. The full details of the RO results for all cases obtained from WAVE are presented in the supplementary materials S.4.

Fig. 12 provides a breakdown of the capital costs associated with the baseline VAWT-CAES-RO system configuration (Case 16), which includes three VAWTs and a PX. The total capital cost for this configuration is about 61,000 US\$. The cost of the individual components is further detailed in Table 3. The most significant cost component is the wind turbines, accounting for 32 % of the total capital cost. This is followed by installation and infrastructure costs, which make up 23 % of the total. The pressure exchanger contributes 13 % to the overall cost. Air-operated HP pump constitutes 19 % of the capital cost, reflecting their importance in pressurising the water for reverse osmosis. The compressed air tank, essential for energy storage, accounts for 6 %. The remaining components, including pre/post-treatment units, RO membranes, and air compressors, each contribute a relatively small percentage (3 % or less) to the overall cost.

Table 4 compares the technical and economic characteristics of the studied cases, highlighting the differences between those without a pressure exchanger (Cases 1–15) and those with one (Cases 16–28). Technically, the number of VAWTs increases from 1 to 15 in Cases 1–15 and from 3 to 15 in Cases 16–28. While the pressure exchanger is absent

# Baseline Configuration Capital Cost (3 VAWTs + PX) = 61K US\$

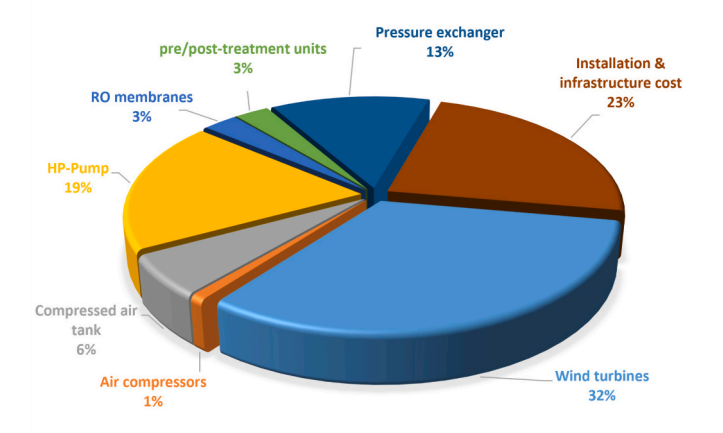


Fig. 12. Capital cost breakdown (%) for the baseline VAWT-CAES-RO system (Case 16: 3 VAWTs + PX).

in Cases 1–15, it is present in Cases 16–28. The changing configurations between Cases 1–15 and Cases 4–10 lead to variations in feed water flow rates, which impact the performance of the RO membranes. For this reason, two types of RO membranes were selected to ensure an optimal recovery ratio: SW30–4040 for the lower feed water rate in Cases 1–15 and SW30XLE-400 for the higher feed water rate in Cases 16–28.

Annual water production is significantly higher in Cases 16–28, ranging from 2554 to  $10,200~\text{m}^3$ , compared to 223 to 2190 m³ in Cases 1–15. The normalised daily water production per square metre of turbine swept area in the optimal case at the study site is approximately  $0.19~\text{m}^3/\text{m}^2/\text{day}$  at an average wind speed of 5 m/s when using the PX, compared to  $0.05~\text{m}^3/\text{m}^2/\text{day}$  when no PX is used.

The most critical distinction lies in the levelised cost of water (LCOW). Cases 1–15 have a higher LCOW range (18–5.5 US\$/m³) compared to the 3–1.63 US\$/m³ range of Cases 16–28, highlighting the economic advantage of the PX. Although the capital costs for Cases 16–28 are higher due to the additional VAWTs and the PX, the significant reduction in LCOW outweighs this initial investment. Overall, the presence of a pressure exchanger in Cases 16–28 significantly improves water production and lowers the levelised cost of water despite the higher initial capital costs. This table emphasises the importance of energy recovery systems in enhancing the efficiency and economic viability of the desalination process.

#### 3.4. Effect of air compressor size on system performance

The size of the air compressor is a critical factor influencing production costs. This section investigates the impact of varying air compressor sizes on the overall performance of the VAWT-CAES-RO system. By analysing different displacement volumes, the impact of different air compressor sizes on key performance metrics was examined. Table 5 summarises the results of a parametric study evaluating the influence of different air compressor displacement volumes (V1 to V4) on system performance. The table includes the LCOW and operational rotor speed ranges for each displacement volume required to achieve the necessary torque for the air compressor.

As the displacement volume increases from V1 to V3, there is a reduction in LCOW. However, further increasing the displacement volume to (V4) leads to a rise in LCOW to  $2.8~\text{US}\text{s/m}^3$ . This increase is due to the greater torque required by the larger compressor, requiring higher wind speeds that are less frequently available at the study location. Thus, while larger displacement volumes can improve system

 Table 4

 Summary of the technical and economical characteristics of all studied cases.

Name	Case 1-15	Case 16-28
Technical values:		
Number of VAWTs	1–15	3-15
Number of Pressure exchanger	0	1
Type of RO membrane	SW30-4040	SW30XLE-400
Number of RO membranes	2	2
Total Active area (m <sup>2</sup> )	14.7	74.3
Annual water Production (m <sup>3</sup> )	223-2190	2554 - 10,200
Avg. daily production (m <sup>3</sup> /day)	0.61-6	7–28
Permeate/swept area (m <sup>3</sup> /m <sup>2</sup> /day)	0.05-0.03	0.19-0.15
Feed water rate (m <sup>3</sup> /h)	1.3	5.79
Recovery rate (%)	20.50	21.65
Feed water TDS (mg/L)	42,200	42,200
Permeate TDS (mg/L)	268	172.6
Avg. flux (LMH)	17.1	16.1
Feed water pressure (bar)	48	48
Air pressure (bar)	7.5	7.5
Economical values:		
levelised cost of water (US\$/m3)	18-5.5	3-1.63
Capital cost (US\$)	31,000 - 152,000	61,000 - 164,000
Annual (O&M) costs (US\$)	1100 - 2100	2100 - 3500
System lifetime (–)	25 Years	
Discount rate (%)	8	

 $\begin{tabular}{ll} \textbf{Table 5} \\ \textbf{Impact of varying air compressor displacement volumes (V1 to V4) on the VAWT-CAES-RO system.} \end{tabular}$ 

	V1	V2 (baseline)	V3	V4
Displacement Volume [m <sup>3</sup> ] LCOW [US\$/m <sup>3</sup> ]	0.0684 5	0.1367 3	0.2734 2.6	0.3175 2.8
Rotor Speeds [RPM]	80-425	115-390	160-340	180-320

performance up to a certain point, excessively large volumes may result in diminishing returns due to the mismatch between the required and available wind conditions.

### 3.5. Effect of transmission ratio on system performance

To investigate the impact of transmission ratios on the performance of a VAWT-driven CAES-RO system, a parametric study was conducted, as presented in Table 6. The table presents the results of a parametric study investigating the impact of different transmission ratios on the system's performance. Four distinct transmission ratios (R1 to R4) were examined to understand how variations in transmission affect the LCOW and the operational rotor speed ranges required to generate the necessary torque for the air compressor.

The results indicate that increasing the transmission ratios initially decreases the LCOW, as observed from R1 to R3. This trend suggests that higher ratios enhance the system's efficiency up to a certain point. However, as the transmission ratio continues to increase, as in R4, the LCOW begins to rise again. This increase is attributed to the higher torque demand, which requires significantly higher wind speeds for maintaining efficient operation. Given the infrequency of such wind speeds at the studied location, the effectiveness of further increasing the transmission ratio beyond a certain threshold was diminished. Understanding these effects is crucial for optimising the system design to ensure cost-effective and reliable water production under varying environmental conditions.

# 3.6. Comparison of the current study to other systems in the literature

The current configuration is compared with similar systems that are off-grid, small to medium scale RO units powered by renewable energy as shown in Table 7. This comparison highlights several factors, including system technologies (Wind and PV), types of connection (electrical and mechanical), salinity and capacities, all of which can significantly influence the levelised cost of water (LCOW). The LCOW for the electrical connection small to medium scale Wind-RO systems in the studies [6,65] ranges from 2.96 to 7.70 US\$/m $^3$  with varying water production rates.

In contrast, for mechanically coupled systems, Liu [77] estimated the LCOW of Wind-RO system at  $1.3~\rm US\$/m^3$  for brackish water desalination. This finding suggests that mechanical connections offer a more cost-effective solution compared to electrical connection. However, more studies of this nature are needed for seawater desalination, as Liu's study focused on brackish water, which typically requires less energy to desalinate than seawater [78]. Mechanical connections have demonstrated their effectiveness in several studies [12,13,19,21,25], but economic assessments were not performed in these studies.

As shown in Table 7, studies on PV-RO systems [79,80] demonstrate a decrease in LCOW with increasing plant capacity. While these studies

 $\begin{tabular}{ll} \textbf{Table 6} \\ \textbf{Impact of varying transmission ratios (R1 to R4) on the VAWT-CAES-RO system.} \\ \end{tabular}$ 

	R1	R2 (baseline)	R3	R4
Transmission Ratio [-]	01:03	01:07	01:15	01:20
LCOW [US\$/m³]	5.6	3	2.6	2.8
Rotor Speeds [RPM]	75–430	115–390	170–340	255–310

**Table 7**Comparison of this study to other small-scale RO system.

Ref.	Technology	LCOW [US \$/m <sup>3</sup> ]	Production [m³/day]	Feed water TDS [mg/L]
This study	Wind-RO (MC)	1.63–3	28–7	42,200
Liu, (2009) [77]	Wind-RO (MC)	1.43	1.33	3000 <sup>a</sup>
Gökçek et al. (2016) [65]	Wind-RO (EC)	2.96-6.46	24	37,865
IRENA, (2015) [6]	Wind-RO (EC)	4.20-7.70	250	-
Mokheimer et al., (2013) [82]	Wind-PV- RO (EC)	3.7–3.8	5	_a
Ayou et al., (2022) [53]	PV-RO (EC)	9	11.6	32,000
Bilton et al. (2011) [81]	PV-RO (EC)	4.96–7.01	9	32,664–41,160
Mostafaeipour et al., (2019) [79]	PV-RO (EC)	1.96–3.02	228–148	39,600
Al-Buraiki et al. [80]	PV-RO (EC)	1.88-2.89	250	40,000

(EC: Electrical connection) (MC: Mechanical Connection).

report LCOW values of  $1.88-3.02~\text{US}\text{s/m}^3$ , the current study achieves a similar LCOW despite a smaller plant capacity, emphasising the potential for cost-effective desalination even at smaller scales. In the other two small-scale PV-RO studies [53,81], the production rates (9–11.6 m³/day) are quite similar to the current study, but the LCOW (4.96–9 US \$/m³) is significantly higher.

A hybrid Wind-PV-RO system [82], with a production of 5 m³ per day, has a slightly higher LCOW of 3.75 US\$/m³ compared to the current study. However, the current system's simplicity is a significant advantage, making it more suitable for the targeted communities with limited resources and technical expertise. This suggests that systems with electrical connections face higher costs, primarily due to the initial investment and maintenance of electrical components and battery storage systems, as well as efficiency losses during energy conversion and storage.

# 4. Conclusion

This study presents a novel, battery-free vertical axis wind turbine-compressed air energy storage-reverse osmosis (VAWT-CAES-RO) system as a feasible and sustainable solution for desalination in remote communities. By mechanically coupling VAWT to a CAES system, the need for costly batteries with shorter lifespans is eliminated, offering a promising pathway to address water scarcity in a cost-effective and eco-friendly manner.

A total of 28 system configurations were investigated to assess the potential of a VAWT-driven CAES system for RO desalination, revealing the significant influence of the design parameters, such as the number of VAWTs and the inclusion of a pressure exchanger (PX), on the system performance and levelised cost of water (LCOW). Importantly, the inclusion of a PX significantly enhances energy recovery, leading to substantial reductions in LCOW. The most cost-effective configuration, employing eleven VAWTs and a PX, achieves an LCOW of 1.63 US\$/m³ and an annual water production of almost 9400 m³. The normalised daily water production per square metre of turbine swept area at the study site is 0.19 m³/m²/day at an average wind speed of 5 m/s.

This comprehensive study establishes the technical feasibility and economic viability of the VAWT-CAES-RO system, showcasing its potential to address the challenges of wind energy intermittency and provide sustainable water solutions for underserved communities. The findings represent a significant advancement in renewable energy-

a brackish water.

driven desalination technologies, offering a practical and cost-effective pathway towards meeting the water needs in a resilient and environmentally conscious manner.

# **Declaration of competing interest**

The authors declare that they have no known competing financial interests or personal relationships that could have appeared to influence the work reported in this paper.

#### Acknowledgments

The first author would like to acknowledge the support of Taif University, Saudi Arabia, for their financial support during his PhD studies. This work was also supported by a Newton Institutional Links grant, ID 527071841. The grant is funded by the UK Department for Business, Energy and Industrial Strategy (BEIS) and the Egypt Science and Technological Development Fund (STDF) and delivered by the British Council.

# Appendix A. Supplementary data

Supplementary data to this article can be found online at https://doi.org/10.1016/j.desal.2024.118094.

#### References

- Unesco World Water Assessment Programme, The United Nations World Water Development Report 2024: water for prosperity and peace, 2024. https://unesdocunesco.org/ark:/48223/pf0000388948 (accessed June 30, 2024).
- [2] S. Schär, A. Bischi, A. Baccioli, U. Desideri, J. Geldermann, Optimization of sustainable seawater desalination: modeling renewable energy integration and energy storage concepts, Energ. Conver. Manage. 293 (2023) 117447, https://doi org/10.1016/j.enconman.2023.117447.
- [3] UNICEF, Reimagining WASH, Water Security for All, https://www.unicef.org/reports/reimagining-wash-water-security-for-all, 2021. (Accessed 30 June 2024).
- [4] G. Baggio, M. Qadir, V. Smakhtin, Freshwater availability status across countries for human and ecosystem needs, Sci. Total Environ. 792 (2021) 148230, https:// doi.org/10.1016/j.scitotenv.2021.148230.
- [5] H.E.M. George-Williams, D.V.L. Hunt, C.D.F. Rogers, Sustainable water infrastructure: visions and options for sub-Saharan Africa, Sustainability 16 (2024) 1592, https://doi.org/10.3390/su16041592.
- [6] IRENA, Renewable Desalination: Technology Options for Islands, Renewable Desalination: Technology Options for Islands (2015) 1–69.
- [7] J. Eke, A. Yusuf, A. Giwa, A. Sodiq, The global status of desalination: an assessment of current desalination technologies, plants and capacity, Desalination 495 (2020) 114633, https://doi.org/10.1016/j.desal.2020.114633.
- [8] Z.M. Ghazi, S.W.F. Rizvi, W.M. Shahid, A.M. Abdulhameed, H. Saleem, S.J. Zaidi, An overview of water desalination systems integrated with renewable energy sources, Desalination 542 (2022) 116063, https://doi.org/10.1016/j. desal.2022.116063.
- [9] S. Alqaed, J. Mustafa, F.A. Almehmadi, Design and energy requirements of a photovoltaic-thermal powered water desalination Plant for the Middle East, Int. J. Environ. Res. Public Health 18 (2021) 1001, https://doi.org/10.3390/ jierph18031001
- [10] J. Bundschuh, M. Kaczmarczyk, N. Ghaffour, B. Tomaszewska, State-of-the-art of renewable energy sources used in water desalination: present and future prospects, Desalination 508 (2021) 115035, https://doi.org/10.1016/j.desal.2021.115035.
- [11] M.A. Abdelkareem, M. El Haj Assad, E.T. Sayed, B. Soudan, Recent progress in the use of renewable energy sources to power water desalination plants, Desalination 435 (2018) 97–113, https://doi.org/10.1016/j.desal.2017.11.018.
- [12] F. Greco, D. de Bruycker, A. Velez-Isaza, N.F.B. Diepeveen, A. Jarquin-Laguna, Preliminary design of a hydraulic wind turbine drive train for integrated electricity production and seawater desalination, J. Phys. Conf. Ser. 1618 (2020) 032015, https://doi.org/10.1088/1742-6596/1618/3/032015.
- [13] D. Keisar, V. Freger, D. Greenblatt, Direct wind-powered vertical axis brackish water desalination system, Desalination 570 (2024) 117060, https://doi.org/ 10.1016/j.desal.2023.117060.
- [14] W. Lai, Q. Ma, H. Lu, S. Weng, J. Fan, H. Fang, Effects of wind intermittence and fluctuation on reverse osmosis desalination process and solution strategies, Desalination 395 (2016) 17–27, https://doi.org/10.1016/j.desal.2016.05.019.
- [15] F. Greco, S. Heijman, A. Jarquin-Laguna, Integration of wind energy and desalination systems: a review study, Processes 9 (2021) 2181, https://doi.org/ 10.3390/pr9122181
- [16] A.H. Alami, A. Yasin, R. Alrashid, S. Alasad, H. Aljaghoub, G. Alabsi, L. Alketbi, A. Alkhzaimi, A. Alteneji, S. Shikhli, Experimental evaluation of compressed air energy storage as a potential replacement of electrochemical batteries, J Energy Storage 54 (2022) 105263, https://doi.org/10.1016/j.est.2022.105263.

[17] S. Orangi, N. Manjong, D.P. Clos, L. Usai, O.S. Burheim, A.H. Strømman, Historical and prospective lithium-ion battery cost trajectories from a bottom-up production modeling perspective, J Energy Storage 76 (2024) 109800, https://doi.org/ 10.1016/j.est.2023.109800

- [18] A. Parschau, D. Degler, A. Fill, K.P. Birke, F. Allmendinger, Cycle tests on the influence of different charging currents—a case study on different commercial, Cylindrical Lithium Ion Cells, Batteries 9 (2023) 83, https://doi.org/10.3390/ https://doi.org/10.3390/
- [19] A. Jarquin-Laguna, F. Greco, Integration of Hydraulic Wind Turbines for Seawater Reverse Osmosis Desalination, in: 2019 Offshore energy and storage summit (OSES), IEEE, 2019: pp. 1–9. doi:https://doi.org/10.1109/OSES.2019.8867343.
- [20] C.C.K. Liu, W. Xia, J.W. Park, A wind-driven reverse osmosis system for aquaculture wastewater reuse and nutrient recovery, Desalination 202 (2007) 24–30, https://doi.org/10.1016/j.desal.2005.12.034.
- [21] S.G.J. Heijman, E. Rabinovitch, F. Bos, N. Olthof, J.C. van Dijk, Sustainable seawater desalination: stand-alone small scale windmill and reverse osmosis system, Desalination 248 (2009) 114–117, https://doi.org/10.1016/j. desal.2008.05.045.
- [22] C. Generaal, Wind Driven Reverse Osmosis Desalination for Small Scale Stand-Alone Applications, Master thesis, TU Delft, 2011. http://resolver.tudelft.nl/uuid :7cb0b53c-4218-4502-b872-1ff5306c757e (accessed July 7, 2024).
- [23] T. Witte, S. Siegfriedsen, M. El-Allawy, WindDeSalter® technology Direct use of wind energy for seawater desalination by vapour compression or reverse osmosis, Desalination 156 (2003) 275–279, https://doi.org/10.1016/S0011-9164(03) 00358-8.
- [24] R. Robinson, G. Ho, K. Mathew, Development of a reliable low-cost reverse osmosis desalination unit for remote communities, Desalination 86 (1992) 9–26, https:// doi.org/10.1016/0011-9164(92)80020-A.
- [25] D. Keisar, B. Eilan, D. Greenblatt, High pressure vertical Axis wind pump, J. Fluids Eng. 143 (2021), https://doi.org/10.1115/1.4049692.
- [26] E. Ali, M. Bumazza, A. Eltamaly, S. Mulyono, M. Yasin, Optimization of wind driven RO Plant for Brackish Water Desalination during wind speed fluctuation with and without battery, MDPI 11 (2021) 77, https://doi.org/10.3390/ membranes11020077.
- [27] P. Cabrera, J.A. Carta, J. González, G. Melián, Wind-driven SWRO desalination prototype with and without batteries: a performance simulation using machine learning models, Desalination 435 (2018) 77–96, https://doi.org/10.1016/j. desal.2017.11.044.
- [28] M. Thomson, D. Infield, Laboratory demonstration of a photovoltaic-powered seawater reverse-osmosis system without batteries, Desalination 183 (2005) 105–111, https://doi.org/10.1016/j.desal.2005.03.031.
- [29] R. Ramkissoon, K. Manohar, A.A. Adeyanju, Small scale wind powered reverse osmosis plant without batteries in Trinidad and Tobago, International Journal of Engineering Trends and Technology 58 (2018) 123–129, https://doi.org/ 10.14445/22315381/JJETT-V58P224.
- [30] A.M. Thomson, Reverse-Osmosis Desalination of Seawater Powered by Photovoltaics without Batteries by, Loughborough University, 2003. https://hdl.ha ndle.net/2134/10701 (accessed June 30, 2024).
- [31] W. Khiari, M. Turki, J. Belhadj, Power control strategy for PV/wind reverse osmosis desalination without battery, Control. Eng. Pract. 89 (2019) 169–179, https://doi.org/10.1016/j.conengprac.2019.05.020.
- [32] Marcos dos Santos Miranda, Small-Scale Wind Powered Seawater Desalination without Batteries, Doctoral Thesis, Loughborough University, 2003. https://hdl.ha ndle.net/2134/10708 (accessed July 7, 2024).
- [33] A. Tummala, R.K. Velamati, D.K. Sinha, V. Indraja, V.H. Krishna, A review on small scale wind turbines, Renew. Sustain. Energy Rev. 56 (2016) 1351–1371, https://doi.org/10.1016/j.rser.2015.12.027.
- [34] L. Du, G. Ingram, R.G. Dominy, A review of H-Darrieus wind turbine aerodynamic research, proc Inst Mech Eng C J Mech, Eng. Sci. 233 (2019) 7590–7616, https://doi.org/10.1177/0954406219885962.
- [35] S. Le Fouest, K. Mulleners, Optimal blade pitch control for enhanced vertical-axis wind turbine performance, Nat. Commun. 15 (2024) 2770, https://doi.org/ 10.1038/s41467-024-46988-0
- [36] C. Wang, P. Meng, S. Wang, D. Song, Y. Xiao, Y. Zhang, Q. Ma, S. Liu, K. Wang, Y. Zhang, Comparison of two types of energy recovery devices: pressure exchanger and turbine in an island desalination project case, Desalination 533 (2022) 115752, https://doi.org/10.1016/j.desal.2022.115752.
- [37] Photovoltaic Geographical Information System, European Commission. https://re.jrc.ec.europa.eu/pvg\_tools/en/, 2020. (Accessed 22 January 2024).
- [38] M.O.L. Hansen, Aerodynamics of Wind Turbines, second edition, 2 ed, Earthscan, 2008.
- [39] R.A.G. Smits, Analysis of a Wind Driven Reverse Osmosis Desalination System Experimental Study, Master thesis, Delft University of Technology, 2019. http://re solver.tudelft.nl/uuid:94973538-dd8f-4a93-8ddd-bb6c7b04522e (accessed July 7, 2024).
- [40] M. Raciti Castelli, G. Ardizzon, L. Battisti, E. Benini, G. Pavesi, Modeling Strategy and Numerical Validation for a Darrieus Vertical Axis Micro-Wind Turbine, in: Volume 7: Fluid Flow, Heat Transfer and Thermal Systems, Parts A and B, ASMEDC, 2010, pp. 409–418, https://doi.org/10.1115/IMECE2010-39548.
- [41] A. Bianchini, F. Balduzzi, G. Ferrara, L. Ferrari, G. Persico, V. Dossena, L. Battisti, Detailed analysis of the wake structure of a straight-blade H-Darrieus wind turbine by means of wind tunnel experiments and computational Fluid dynamics simulations, J Eng Gas Turbine Power 140 (2018) 1–9, https://doi.org/10.1115/ 1.4037906.
- [42] L. Battisti, G. Persico, V. Dossena, B. Paradiso, M. Raciti Castelli, A. Brighenti, E. Benini, Experimental benchmark data for H-shaped and troposkien VAWT

- architectures, renew, Energy 125 (2018) 425-444, https://doi.org/10.1016/j.
- [43] Bambi air, Bambi Oil Free Air Compressor, BAMBI AIR LTD (n.d.). https://bambi-air.co.uk/ (accessed July 7, 2024).
- [44] Heinz P. Bloch, John J. Hoefner, Reciprocating Compressors, Elsevier (1996), https://doi.org/10.1016/B978-0-88415-525-6.X5000-7.
- [45] Air Link Compressors, 2000Ltr Vertical Compressed Air Receiver Tank. https://airlinkcompressors.com/products/painted-vertical-compressed-air-receiver-tank-2000l-fittings-4101000928, 2024. (Accessed 10 June 2024).
- [46] DuPont, FilmTec™ Reverse Osmosis Membranes Technical Manual (2023). htt ps://www.dupont.com/content/dam/dupont/amer/us/en/water-solutions/publi c/documents/en/RO-NF-FilmTec-Manual-45-D01504-en.pdf (accessed July 7, 2024)
- [47] I. Rand Company, Operator's Manual & Sales and Engineering Data: AF807MXXXXXX-XX-X Four-Ball Pump Series. www.ingersollrandproducts.com, 2010
- [48] E. Tzen, D. Theofilloyianakos, Z. Kologios, Autonomous reverse osmosis units driven by RE sources experiences and lessons learned, Desalination 221 (2008) 29–36. https://doi.org/10.1016/j.desal.2007.02.048.
- [49] I. Ben Ali, M. Turki, J. Belhadj, X. Roboam, Systemic design and energy management of a standalone battery-less PV/wind driven brackish water reverse osmosis desalination system, Sustain Energy Technol Assess 42 (2020) 100884, https://doi.org/10.1016/j.seta.2020.100884.
- [50] J.A. Carta, J. González, P. Cabrera, V.J. Subiela, Preliminary experimental analysis of a small-scale prototype SWRO desalination plant, designed for continuous adjustment of its energy consumption to the widely varying power generated by a stand-alone wind turbine, Appl. Energy 137 (2015) 222–239, https://doi.org/ 10.1016/j.japenergy.2014.09.093.
- [51] L. Fortunato, A.H. Alshahri, A.S.F. Farinha, I. Zakzouk, S. Jeong, T. Leiknes, Fouling investigation of a full-scale seawater reverse osmosis desalination (SWRO) plant on the Red Sea: membrane autopsy and pretreatment efficiency, Desalination 496 (2020) 114536, https://doi.org/10.1016/j.desal.2020.114536.
- [52] M.M. Zubair, H. Saleem, S.J. Zaidi, Recent progress in reverse osmosis modeling: an overview, Desalination 564 (2023), https://doi.org/10.1016/j.
- [53] D.S. Ayou, H.M. Ega, A. Coronas, A feasibility study of a small-scale photovoltaic-powered reverse osmosis desalination plant for potable water and salt production in Madura Island: a techno-economic evaluation, Thermal Science and Engineering Progress 35 (2022) 101450, https://doi.org/10.1016/j.tsep.2022.101450.
- [54] N. Ahmad, A.K. Sheikh, P. Gandhidasan, M. Elshafie, Modeling, simulation and performance evaluation of a community scale PVRO water desalination system operated by fixed and tracking PV panels: a case study for Dhahran city, Saudi Arabia, renew, Energy 75 (2015) 433–447, https://doi.org/10.1016/j. renene.2014.10.023.
- [55] M.W. Haefner, M.N. Haji, Integrated pumped hydro reverse osmosis System optimization featuring surrogate model development in reverse osmosis modeling, Appl. Energy 352 (2023). https://doi.org/10.1016/j.apenergy.2023.121812.
- [56] J.G. Wijmans, R.W. Baker, The solution-diffusion model: a review, J Memb Sci 107 (1995) 1–21, https://doi.org/10.1016/0376-7388(95)00102-I.
- [57] DuPont, Water Application Value Engine (WAVE), FilmTec. https://www.dupont.com/water/resources/design-software.html, 2024. (Accessed 7 July 2024).
- [58] Energy Recovery, PX S Series PX 30 Pressure Exchanger. https://energyrecovery.com/desalination/high-pressure-px/, 2023. (Accessed 7 July 2024).
   [59] Energy recovery, Water Products Catalog. https://energyrecovery.com/resources
- [59] Energy recovery, Water Products Catalog. https://energyrecovery.com/resources/water-products-catalog/, 2024. (Accessed 7 July 2024).
- [60] J. Zhou, D. Liu, Q. Zhang, F. Wang, Y. Liu, C. Bian, X. Wang, X. Meng, N. Yang, Investigations on the energy conversion and dissipation in hydraulic-driven rotary energy recovery device from a designer's perspective: simulation and validation, Desalination 563 (2023) 116718, https://doi.org/10.1016/j.desal.2023.116718.
- [61] Power Model Pro, Energy Recovery. https://energyrecovery.com/resources/p ower-model-pro/, 2024. (Accessed 8 July 2024).

- [62] Topflo, Air operated diaphragm pumps, n.d. https://tapflo.com/en/ (accessed July 11, 2024).
- [63] DuPont, FilmTec™ SW30 Seawater RO Elements for Commercial Systems. https://www.dupont.com/content/dam/dupont/amer/us/en/water-solutions/public/documents/en/RO-FilmTec-SW30-Seawater-PDS-45-D01519-en.pdf, 2023. (Accessed 7 July 2024).
- [64] DuPont, FilmTecTM™ SW30XLE-400 Seawater Low Energy Reverse Osmosis Membrane Element. https://www.dupont.com/content/dam/dupont/amer/us/en/water-solutions/public/documents/en/RO-FilmTec-SW30XLE-400-P DS-45-D00972-en.pdf, 2022. (Accessed 7 July 2024).
- [65] M. Gökçek, Ö.B. Gökçek, Technical and economic evaluation of freshwater production from a wind-powered small-scale seawater reverse osmosis system (WP-SWRO), Desalination 381 (2016) 47–57, https://doi.org/10.1016/j. desal.2015.12.004.
- [66] Aeolos, Aeolos Wind Energy Ltd, (n.d.). https://www.windturbinestar.com/ (accessed June 29, 2024).
- [67] Aeolos, Wind Turbine EXW Price List V-series Wind turbines, 2019.
- [68] Compressor Shop, MK102 Belt Driven Pump. https://www.compressorshop.co. uk/mk102-belt-driven-pump, 2024. (Accessed 29 June 2024).
- [69] A.R.O. Fluid Management, AF0807 Series 4-Ball Piston Pumps. https://www.arozone.com/en-ua/piston-pumps/af0807, 2024. (Accessed 10 June 2024).
- [70] Flexible Assembly Systems Inc, ARO AF0807M11KS48 | CF8M SS 4-Ball Piston Pump. https://www.flexibleassembly.com/Ingersoll-Rand-AF0807M11KS48-7-1-R atio-Four-Ball-Piston-Pump, 2024. (Accessed 29 June 2024).
- [71] Pumps Direct, Air-Operated Double Diaphragm Pump. https://www.pumpsdirect. com/graco-husky-716-3-4-air-operated-double-diaphragm-pump-d5c366, 2024. (Accessed 10 June 2024).
- [72] Big Brand Water Filter Inc, DOW Filmtec SW30-4040 RO Membrane. https://www.bigbrandwater.com/sw30-4040.html, 2024. (Accessed 29 June 2024).
- [73] Big Brand Water Filter Inc, DOW Filmtec SW30XLE-400i RO Membrane. https://www.bigbrandwater.com/sw30xle-400i.html, 2024. (Accessed 29 June 2024).
- [74] M. Monnot, G.D.M. Carvajal, S. Laborie, C. Cabassud, R. Lebrun, Integrated approach in eco-design strategy for small RO desalination plants powered by photovoltaic energy, Desalination 435 (2018) 246–258, https://doi.org/10.1016/j. desal.2017.05.015.
- [75] K.H. Mistry, J.H. Lienhard V., An economics-based second law efficiency, Entropy 15 (2013) 2736–2765. https://doi.org/10.3390/e15072736.
- [76] V.K. Rao, P.S. Murty, M.S. Reddy, S.A. Sundaresan, Study of accelerating torque requirements of a reciprocating compressor, in: International Compressor Engineering Conference, 1996. https://docs.lib.purdue.edu/icec/1083. (Accessed 25 June 2024).
- [77] C.C.K. Liu, Wind-Powered Reverse Osmosis Water Desalination for Pacific Islands and Remote Coastal Communities, U.S. Department of the Interior, Bureau of Reclamation, 2009.
- [78] H. Kariman, A. Shafieian, M. Khiadani, Small scale desalination technologies: A comprehensive review, Desalination 567 (2023) 116985, https://doi.org/10.1016/ i.desal.2023.116985.
- [79] A. Mostafaeipour, M. Qolipour, M. Rezaei, E. Babaee-Tirkolaee, Investigation of off-grid photovoltaic systems for a reverse osmosis desalination system: a case study, Desalination 454 (2019) 91–103, https://doi.org/10.1016/j. desal.2018.03.007.
- [80] A.S. Al-Buraiki, A. Al-Sharafi, M.A. Antar, Excess energy recovery from a standalone PV system for freshwater production using RO unit: techno-economic analysis, Desalination 586 (2024), https://doi.org/10.1016/j.desal.2024.117824.
- [81] A.M. Bilton, R. Wiesman, A.F.M. Arif, S.M. Zubair, S. Dubowsky, On the feasibility of community-scale photovoltaic-powered reverse osmosis desalination systems for remote locations, renew, Energy 36 (2011) 3246–3256, https://doi.org/10.1016/j. renepe.2011.03.040.
- [82] E.M.A. Mokheimer, A.Z. Sahin, A. Al-Sharafi, A.I. Ali, Modeling and optimization of hybrid wind-solar-powered reverse osmosis water desalination system in Saudi Arabia, Energ. Conver. Manage. 75 (2013) 86–97, https://doi.org/10.1016/j. enconman.2013.06.002.